scientific reports

Check for updates

OPEN

Rapid prototyping of thermoplastic microfluidic devices via SLA 3D printing

Harrison Khoo[1], William Shaen Allen[2], Netzahualcóyotl Arroyo-Currás[3,4] & Soojung Claire Hur[1,4,5]✉

Microfluidic devices have immense potential for widespread community use, but a current bottleneck is the transition from research prototyping into mass production because the gold standard prototyping strategy is too costly and labor intensive when scaling up fabrication throughput. For increased throughput, it is common to mold devices out of thermoplastics due to low per-unit costs at high volumes. However, conventional fabrication methods have high upfront development expenses with slow mold fabrication methods that limit the speed of design evolution for expedited marketability. To overcome this limitation, we propose a rapid prototyping protocol to fabricate thermoplastic devices from a stereolithography (SLA) 3D printed template through intermediate steps akin to those employed in soft lithography. We apply this process towards the design of self-operating capillaric circuits, well suited for deployment as low-cost decentralized assays. Rapid development of these geometry- and material-dependent devices benefits from prototyping with thermoplastics. We validated the constructed capillaric circuits by performing an autonomous, pre-programmed, bead-based immunofluorescent assay for protein quantification. Overall, this prototyping method provides a valuable means for quickly iterating and refining microfluidic devices, paving the way for future scaling of production.

Rapid prototyping comprises a set of techniques used to fabricate physical objects or components of a system directly from computer-aided design (CAD) data before the final product is manufactured[1,2]. This pivotal process significantly enhances overall product development by enabling the prediction, evaluation, and iteration of design features, concepts, and operational functionality and performance. The efficiency gained through rapid prototyping accelerates the product development timeline and cost. In the field of microfluidics, the significance of rapid prototyping is prominently exemplified by the advent of soft lithography using polydimethylsiloxane (PDMS)[3]. By leveraging the inherent benefits of miniaturization, the field of microfluidics has demonstrated extensive applications in sample preparation, biosensors, diagnostics, and other interdisciplinary fields within recent decades[4–6]. The ability to allow convenient and cost-effective fabrication of microfluidic systems using polymers has elevated these systems from being marginally impactful in research settings, when manufactured using fabrication steps derived from microelectronics, to being actively explored for their full potentials.

Not surprisingly, there has been a continuous effort to expand the use of microfluidics beyond research settings for a broader audience[7]. In addition to enabling previously-not-possible sophisticated assays in the highly well-structured research setting, the microfluidic community has started translating assays from bench to bedside by simplifying workflows for untrained users. For example, paper-based microfluidics[8,9] and capillaric circuit (CC)[10,11] technologies permit low cost, automated operational capability without the need for auxiliary equipment, highly skilled personnel, or benchtop footprint. CCs, in particular, excel in performing decentralized assays due to their ability to achieve complex deterministic, pre-programmed flows of different reagents into a reaction microchannel[11]. Notably, this is accomplished in CCs without external pumps or pressure sources for on-chip enzyme-linked immunosorbent assays (ELISAs), detecting a variety of antibodies[12,13], proteins[13–17], drugs[18], anions[19], and bacteria[20].

The translation of these technologies necessitates a new rapid prototyping process facilitating uninterrupted transitions to mass production of systems with microscale features[21–23]. Soft lithography using PDMS, the current

[1]Department of Mechanical Engineering, Johns Hopkins University, 3400 N Charles ST., Latrobe 105, Baltimore, MD 21218, USA. [2]Baltimore Polytechnic Institute, Baltimore, MD, USA. [3]Department of Pharmacology and Molecular Sciences, Johns Hopkins University School of Medicine, Baltimore, MD 21205, USA. [4]Institute of NanoBioTechnology, Johns Hopkins University, Baltimore, MD, USA. [5]The Sidney Kimmel Comprehensive Cancer Center, Johns Hopkins Hospital, Baltimore, MD, USA. ✉email: schur@jhu.edu

gold standard rapid prototyping method for microfluidics, seems inadequate to meet the demands of the new wave of microfluidic commercialization due to the high requirements involved in scaling up its production, as increasing manufacturing volume does not significantly reduce individual unit costs due to long processing time[24]. Additive manufacturing with resin-based 3D printing is emerging as an alternative prototyping methodology for microfluidic devices[25,26], but the process is still relatively low throughput due to its layer-by-layer methodology. Nevertheless, it is possible to achieve low-cost, high-volume production of microfluidic devices by using thermoplastics. In industry, microfluidic bioassay cartridges are often molded with thermoplastics using, for example, poly (methyl methacrylate) (PMMA)[22,27], through methods such as hot embossing, injection molding and roll-to-roll imprinting[23,28–30]. The tradeoff for these fabrication techniques is their expensive upfront costs in fabricating molds, which is infeasible when device designs are still being iterated upon. Moreover, the translation of prototyped features from PDMS or 3D printed microfluidic devices into thermoplastic is not seamless. Materials used in microfluidic rapid prototyping exhibit drastically different material and surface properties than rigid thermoplastics[31]. As a result, not all existing geometries and chemistries validated for prototypes in research settings are necessarily transferrable[28]. Lengthy re-optimization processes are unavoidable, inevitably adding to development cost and deployment time. An optimal prototyping method for microfluidic devices with scalable appeal utilizes accessible, low-cost equipment with rapid processing time to produce thermoplastic devices.

In this work, we present an efficient, robust, and inexpensive protocol to rapidly transfer multi-height microscale features from SLA 3D printed molds to hot embossed thermoplastics through a series of intermediate replicates (Fig. 1). The established protocol only utilizes materials that are common in research settings or commercially available at low cost. The fabrication pipeline offers the potential to move from device ideation to final product in less than 48 h, with the total material costs for the entire manufacturing process below $15. We validated the established rapid protocol by constructing CCs capable of performing pre-programmed, autonomous immunofluorescence protein quantification. The proposed fabrication protocol serves as a rapid and practical prototyping strategy, while also considering scalability for downstream production.

Capillaric circuit design

CCs are passive microfluidic devices that enable pre-programmed, time-controlled fluid flow sequences with multiple reagents to perform complex assays on-chip. CCs are composed of multiple components, including retention burst valves (RBVs) and trigger valves (TVs), organized to form branches that facilitate a defined order of fluid flow. Branch depletion order and duration are geometry-sensitive, as CC components are organized to balance capillary pressure (P_c) and hydraulic resistances (R_h), which are reflected by the following governing equations. P_c can be determined by the Young-Laplace equation[11],

$$P_c = -\gamma\left(\frac{\cos\left(\theta_{top}\right)+\cos\left(\theta_{bottom}\right)}{h}+\frac{\cos\left(\theta_{left}\right)+\cos\left(\theta_{right}\right)}{w}\right), \tag{1}$$

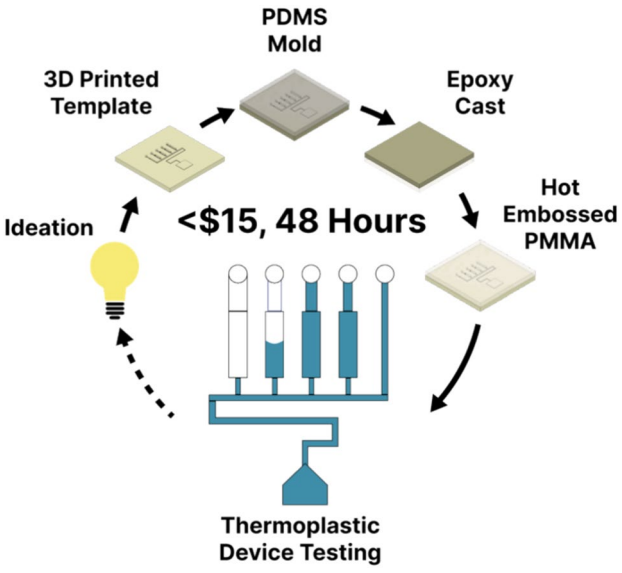

Figure 1. A schematic overview of the proposed rapid fabrication process. After a new channel design is conceptualized, the microscale, multi-height features are produced using an SLA 3D printer. Following sequential PDMS and epoxy casting, the final device is produced in PMMA via hot embossing. Geometries could be iterated quickly based on experimental outcomes. We manufactured and validated CCs using this workflow.

where γ is the surface tension, θ is the contact angle between the fluid and the material of the associated microchannel wall, h is the height of the microchannel and w is the width of the microchannel. R_h of a rectangular channel[11] is represented by

$$R_h = \frac{12\mu L}{wh^3\left(1 - 0.63\left(h/w\right)\right)} \quad (2)$$

where μ represents the fluid viscosity and L represents the microchannel length.

Traditional microfabrication methods historically hindered geometric innovation in CCs due to limited throughput and financial viability, particularly for producing multi-height microscale features using conventional microfabrication methods in microfluidic manufacturing. Recent advancements of CCs leverage additive manufacturing, allowing reliable 3D printing of features with previously unrealizable geometries that enhance CC functionalities without significant additional fabrication complexity. This flexibility enables a wider range of R_h and P_c within the same device footprint. As such, devices have been fabricated using PDMS cast from 3D printed templates[18,20,32] or additive manufacturing directly[12–16,18,19].

Despite significant advancements, the full potential of CCs as powerful, inexpensive and decentralized biological assay kits remains unrealized due to the lack of high-volume production using thermoplastics. One of the limiting factors is that the structural and functional features, currently optimized for the selected substrate materials, must undergo inevitable re-optimization when transitioning from PDMS or 3D printed resins to thermoplastics due to the variations in contact angles, θ Eq. (1). In this study, we decided to validate our rapid prototyping method for thermoplastic CC development, aiming for expedited mass production of CCs as decentralized diagnostic devices.

Materials and methods

Capillaric circuit design

The CC device we designed and constructed consists of multiple CC components, including RBVs, TVs, resistors, and a capillary pump[11]. A circuit diagram was devised for the device layout (SI: Fig. S1), and a Python script was written to calculate the hydraulic resistance and capillary pressure of each component. The sessile drop method was used to estimate the contact angle of water with plasma-treated PMMA (8560K257, McMaster Carr, USA) and pressure-sensitive tape (ARcare 90445Q, Adhesive Research, USA), with image analysis performed using the DropSnake plugin on FIJI[33,34]. Measured contact angles, along with the fluid viscosity of water, were set as constants in Eq. (1) to estimate capillary pressures for each CC component. Feature dimensions were selected that aligned with the 3D printer capabilities (25 μm XY resolution and layer height[35]).

Rapid prototyping protocol

We developed a streamlined rapid prototyping process for constructing thermoplastic devices with microscale features. This method utilized multiple casting steps and materials commonly found in research settings. The sequential processing steps comprise (i) 3D printed template design and construction, (ii) PDMS mold casting, (iii) high-temperature epoxy replication, and (iv) hot embossing thermoplastics. The materials employed in each step are detailed below, along with brief descriptions of their respective roles.

3D printed template

CCs were designed using CAD software (AutoCAD, Autodesk Inc., USA) (SI: Table S1, files available upon request). The CAD design was exported as an STL file and uploaded in the PreForm software to be printed using the Form3 SLA 3D printer (FormLabs, USA) with commercially available, general purpose Clear v4 resin (RS-F2-GPCL-04, FormLabs, USA). After printing, the printed object was sonicated in fresh isopropanol for 5 min to wash away uncured resin and dried. Subsequently, the 3D printed template was baked for 1 h at 120 °C in an oven (Quincy Labs, USA)[36]. The 3D printed object was cooled to 20 °C.

PDMS mold

The 3D printed template was placed in a petri dish and lightly sprayed with an epoxy release spray (Ease Release 200, Mann Release Technologies, USA). It was left to dry for 5 min. Meanwhile, PDMS (Sylgard 184, Dow Corning, USA) was mixed thoroughly at a 10:1 ratio. The PDMS mixture was poured onto the mold and degassed in a vacuum chamber before being cured at 85 ℃ for 1 h. After cooling to room temperature, the cured PDMS was cut to create a positive device mold.

Epoxy cast

The PDMS positive mold was placed in a petri dish and the feature side was sprayed lightly with an epoxy release spray. It was left to dry for 5 min, followed by an additional 5 min of degassing in a vacuum chamber. A two-part, high-temperature epoxy (EpoxAcast 670 HT, Smooth-On, USA) was mixed according to the manufacturer's instructions (100:16 weight ratio of Part A to Part B). Bubbles that formed from mixing were removed via centrifugation (5 min at 1000 RPM) and manual agitation with a 20G needle tip (Instech Laboratories, USA) after casting. The epoxy-filled mold was then cured according to the manufacturer's instructions: 24 h at room temperature (20 ℃), followed by 2 h at 80 ℃, and 3 h at 150 ℃. The epoxy replicate was removed from the PDMS mold after curing for 24 h at 20 ℃. If needed, the base of the epoxy was smoothed using sandpaper (80 grit, Fandeli, Mexico).

Hot embossed PMMA

1/8″ thick acrylic sheets (McMaster Carr, USA) were laser cut (VLS6.60, Universal Laser Systems, USA) into square pieces that were smaller than the epoxy mold dimensions. Of note, the laser cutting can be replaced with a manual handsaw without adversely impacting the manufacturability. The cut PMMA piece was placed on top of the epoxy mold, surrounded by an off-ratio PDMS (20:1) spacer and placed on the lower platen (VEVOR, USA) of a hydraulic shop press (Strongway, USA). The upper platen was then lowered and heated to 140 ℃, and then approximately 500 lb of force was applied for 5 min. The substrate was allowed to cool down to 90 ℃ before the pressure was released. The PMMA was subsequently separated from the epoxy mold using tweezers. Hot embossed PMMA devices were cleaned using tape (Scotch, USA) to remove dust before being O_2 plasma treated (Technics MicroRIE, USA) at 0.3 mbar for 75 s. The device was sealed using precisely cut sealing tape.

Feature dimension measurements

The feature dimensions on the manufactured substrates at various molding steps were characterized using a surface profilometer (VK-X100, Keyence, Japan). Vertical dimensions were measured by determining the vertical distance between a randomly selected location on the base and embossed feature. Horizontal dimensions were measured by focusing the image along the base of each feature and measuring the lateral length at 10 × magnification.

The manufactured features were visually inspected using images taken using a JSM-IT700HR Scanning Electron Microscope (SEM) (Jeol Ltd., USA) at a 15° angle at 45 × magnification. Prior to imaging, substrates were sputtered with a 10 nm thick platinum layer (EM ACE 600, Leica, Germany).

Pre-programmed flow sequence validation

To evaluate the enclosed CC functionality, 1:10 diluted blue food dye (McCormick, USA) in DI water was prepared. The volume of food dye, corresponding to the sum of the associated RBV, reservoir, and TV, was pipetted into branches 1–4 to sufficiently fill each branch. To trigger the reagent flow, 30 µL of diluted food dye (i.e., the wetting solution) was added to the wetting channel inlet. Once the injected wetting solution reached the capillary pump outlet, we inserted a 1 cm wide strip of filter paper (Qualitative filter paper, Grade 1, Whatman, USA) with a 90° angled tip along the designed groove. This action initiated fluid wicking, leading to the activation of the CC. A video was taken of the entire fluid flow process using a smartphone camera (iPhone 14 Pro, Apple Inc., USA).

Immunofluorescence protein quantification assay

Quantification of bovine serum albumin (BSA) was performed to validate this proof-of-concept CC device using anti-BSA antibody-coated polydisperse agarose beads prepared off-chip as a protein-detection packed bead column. Briefly, 40 µL of streptavidin-functionalized agarose beads (Streptavidin Agarose, Millipore Sigma, USA) (diameter 40–165 µm) were diluted in 320 µL PBS (14190250, ThermoFisher Scientific, USA), centrifuged and washed with PBS. Subsequently, beads were incubated in 100 µg/mL biotinylated anti-BSA antibody (A10-113B, ThermoFisher Scientific, USA) for 1 h at 20 ℃. Beads were once again washed with PBS and resuspended in 400 µL PBS. Subsequently, serial dilutions (100 ng/mL–1 mg/mL) of BSA-FITC (A23015, ThermoFisher Scientific, USA) were prepared in PBS to assess the limit of detection.

Branches 1–4 of the CC devices were loaded with a dilution of BSA-FITC or PBS for protein quantification and washing, respectively. The antibody-coated bead solution was resuspended and added to the wetting branch to trigger device flow. A video was taken of the entire flow sequence using a smartphone camera. This video was time stamped to determine the flow time of each branch.

After the remaining 10 µL of the wetting solution flown through the main channel, the device was protected from light and the bead column was imaged on an inverted microscope (Eclipse Ti2, Nikon Inc., Japan) with a light source (SOLA Light Engine, Lumencor, USA), fluorescent filter cubes, and a CCD camera (CoolSNAP DYNO, Photometrics, USA).

Each fluorescence image of the agarose bead detection column was analyzed using ImageJ. Three preset regions of interest (ROI, 300 × 300 px^2) of each bead column were selected at the center of the channel. The mean intensity of each ROI was determined, and the average of these three values comprised one data point. Triplicate experiments at each protein concentration were performed. The same ROIs were used for each image. A four-parameter logistic regression was used to fit an S curve using the generated fluorescence data from the serial dilutions[37,38]. The limit of detection (LOD) was calculated[39] and matched with the S curve to determine the minimum detection concentration.

Results and discussion

Establishment and optimization of the rapid fabrication protocol

Low-cost fabrication and design iteration of thermoplastic devices help expedite the deployment of microfluidic devices for impactful applications. There have been notable recent works expanding the scope of research beyond PDMS prototypes of microfluidic devices. For example, thermoplastic features have been embossed from photolithographic molds via reinforced PDMS molds[40–43] or epoxy[44–49]. Direct laser ablation onto surfaces has been proposed for quick design iteration by tuning laser power to achieve different engraving depths[17,50]. Recent works have begun to utilize additive manufacturing for complex feature design. Lin et al. 3D printed a metal mold for direct hot embossing of thermoplastics[30]. A PolyJet 3D printed mold to thermoplastic fabrication workflow was also recently published[51]. We built on these recent advances to leverage the benefits of designing diverse, multi-height features with additive manufacturing with the fabrication scalability of thermoplastic devices, while further reducing financial burdens, manufacturing time and complexity. The rapid, affordable fabrication protocol was developed by converting SLA 3D printed templates with microscale multi-height features into

planar PMMA replicates (Fig. 2A). Fabrication steps are accomplished using materials and equipment readily available in microfluidic research labs or that can be acquired for low costs. Each stage is optimized to reduce the manual labor and overall processing time.

3D printed template

We utilized an SLA 3D printer with a low capital-expenditure (< $2500) to produce complex, multi-height features. SLA 3D printing has emerged as a widespread engineering tool for in-house prototyping before the product development completion[25,26]. A range of low-cost, easy-to-use options, with resolution down to the tens of microns, are now commercially available. The reliable and autonomous nature of 3D printers ensures high repeatability. Additionally, multiple different geometries can be printed on the same print bed for parallelized testing. Features were designed atop a 4 mm base, which was sufficiently thick to minimize print warping from thin features. The 3D print template could not be used directly as a mold for hot embossing PMMA because the general purpose resin has a relatively low heat deflection temperature (73 ℃ at 0.45 MPa). Hence, the 3D printed part was a template for the intermediate molds.

Utilizing cost-effective resins for constructing the 3D printed template to achieve multi-height microscale features necessitated the identification of an additional replication method suitable as a base for hot embossing thermoplastics. Consequently, we chose PDMS to cast high-temperature epoxy, creating a secondary positive mold for hot embossing. Prior to PDMS molding of the 3D printed template, it was crucial to thoroughly cure the 3D printed object because a common challenge arises in the leeching of residual uncured photoinitiators from the print[36]. This leaching prevents complete curing of the PDMS in the proximity of the print surface, hindering effective feature transfer. For the specific resin we used, the same issue persisted, even with the manufacturer

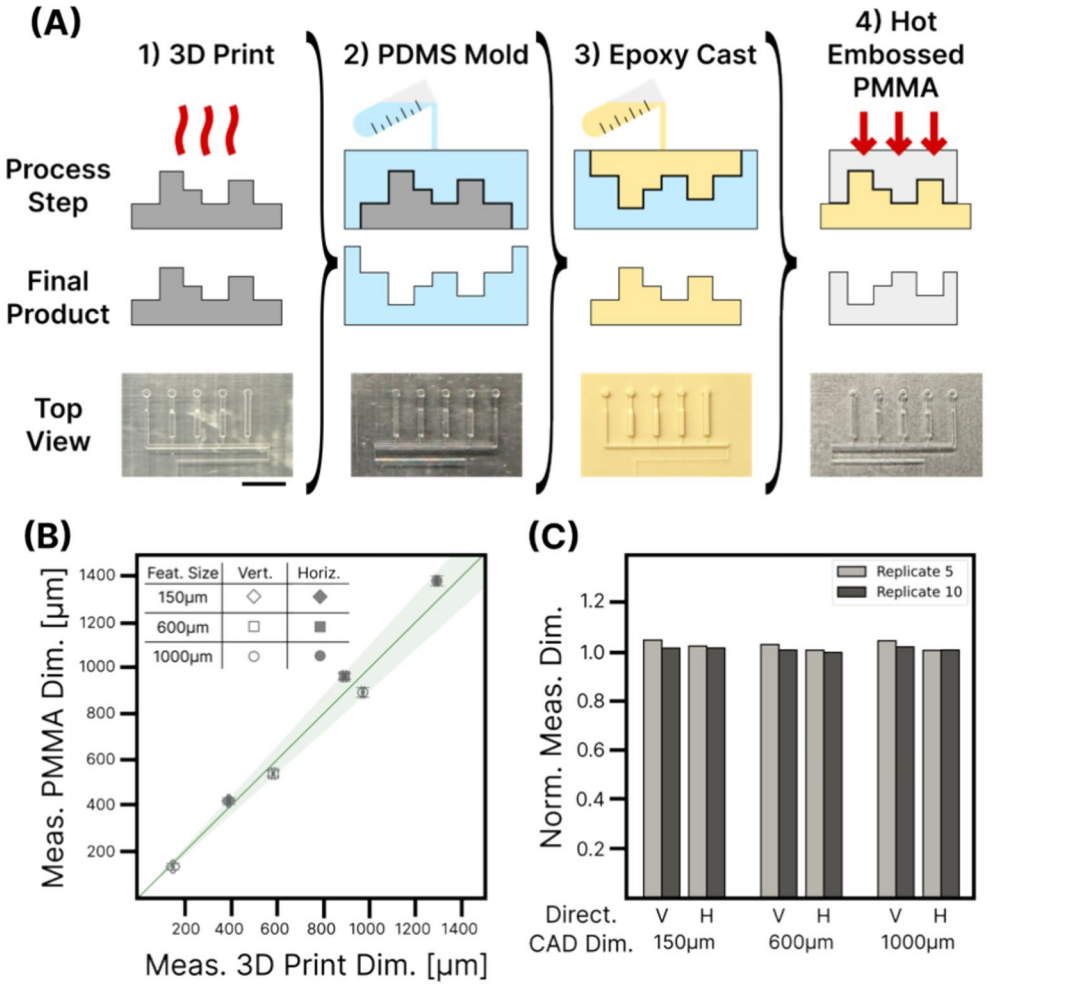

Figure 2. Illustrations of the rapid fabrication process. (**A**) A schematic (Process Step and Final Product) and pictorial (Top View) representation of each fabrication step. Scale bar = 1 cm. (**B**) Comparison of measured vertical and horizontal dimensions of 3D printed and PMMA features. The entire workflow was replicated 3 × to assess process variability. The green line represents the 1:1 dimension match between substrates, with the shaded region representing 10% deviation for a given dimension. (**C**) Vertical (V) and Horizontal (H) dimension comparison between PMMA Replicates 5 and 10, normalized to Replicate 1 using the same epoxy mold.

recommended UV exposure and bake treatment (30 min at 60 °C). Alternative methods, such as coating the print surface, were either cumbersome[52] or time-consuming[53]. We adopted a simple solution by implementing an additional 1 h device bake at high temperatures (120 °C), which was previously optimized for our specific resin formulation[36]. Additionally, a release spray was used to cleanly separate the PDMS from the 3D printed template without altering the features.

Epoxy cast

The cleanly delaminated PDMS replica of the 3D printed template was then used to cast high-temperature epoxy as the base for hot embossing thermoplastics. Drawing inspiration from the use of metal-filled epoxies for robust hot embossing molds[44,51] which, due to their longer curing times and higher viscosity, are still less than ideal for rapid prototyping, we opted for a commercial epoxy exhibiting excellent temperature resistance and relatively low viscosity (6000 cP). Nevertheless, bubbles with similar size ranges to our features formed in the epoxy remained an issue, potentially leading to unintended features in the final product. To address the inevitable bubble formation during the mixing of the two-part epoxy, we subjected the epoxy to a gentle centrifugation (1000 RPM for 5 min) before casting. Additionally, when pouring, larger bubbles could be trapped due to the viscous nature of this epoxy, which did not readily fill PDMS cavities. Employing the common degassing process used in soft lithography, which involves casting the epoxy in a vacuum, proved ineffective in removing bubbles from a mixture more viscous than PDMS. Instead, careful agitation of bubbles with a 20G needle tip was sufficient to dislodge the air bubbles from the features. A small amount of epoxy (< 15 mL), enough to submerge the features, was first poured onto the PDMS mold, and bubbles were agitated. After the surface was free of bubbles, additional epoxy was poured to fill the mold. If the epoxy was slightly underfilled, the edges of the epoxy base formed a raised lip against the PDMS mold after curing and was manually sanded down using coarse sandpaper to ensure a flat surface. The flattened epoxy mold exhibited an improved lifespan since premature mold cracking, caused by uneven mold height during hot embossing, was prevented.

Hot embossed PMMA

We rigorously tested and validated that the high-temperature epoxy mold could withstand the high temperatures and pressures of an embossing cycle on our inexpensive hot embossing setup (< $500) without cracking or significant deformation. Various works have suggested different temperatures, pressures, and time combinations to achieve proper PMMA molding[30,40,49,54]. We determined that applying 500 lb of force for 5 min at 140 ℃ was sufficient for pattern transfer. PMMA devices were separated from the epoxy mold at 90 ℃, below the glass transition temperature of PMMA (T_G = 105 ℃). The placement of a deformable spacer (20:1 PDMS) surrounding the epoxy mold helped to evenly apply compressing force to emboss. Hot embossing without the spacer led to uncontrollable cracking of the epoxy mold.

Feature resolution and reproducibility

We determine the replication resolution limit and reproducibility of the multi-height microscale features produced using our rapid prototyping method through systematic and quantitative measurements and analyses of dimensions. We measured the horizontal and vertical dimensions of various features throughout the fabrication process to assess deviations from the expected feature size and output. Microchannels with square cross-sections (150, 600, 1000 μm) in the designed CC were characterized using an optical profilometer. Figure 2B and SI: Fig. S2 illustrate the variations in feature dimensions as we proceed through the replication process from the 3D printed template to the final PMMA product. Due to the method of measuring dimensions, there were initial deviations between the CAD and 3D printed dimensions (SI: Fig. S3). However, the relative change in feature dimensions from the 3D printed template to the hot embossed PMMA were consistent. Across all three PMMA channels, there was a ~ 10% reduction in height and ~ 7% increase in width relative to the 3D printed feature (Fig. 2B). To determine whether the dimension changes would be further exacerbated with repeated hot embossing steps, ten replicate devices were fabricated from the same epoxy mold. Replicates 1, 5 and 10 were assessed to identify feature dimension changes (Fig. 2C). There were minimal changes in both horizontal (< 5%) and vertical (< 3%) dimensions in Replicates 5 and 10 compared to Replicate 1. Thus, as geometries are finalized and multiple device replicates are needed for downstream experiments, the same epoxy mold may be used for multiple fabrication cycles instead of repeating the entire process. Notably, others have demonstrated the ability to hot emboss thermoplastics using epoxy molds derived from photolithographic molds[44–49]. As a demonstration, additional fabrication cycles were performed using smaller features produced with an expensive PolyJet 3D printed and photolithographic templates, along with PMMA features replicated directly from Form3 printed templates using high temperature resin (SI: Fig. S4). The smaller features were reproduced in PMMA with similar deviations (< 10%) to those produced from the Form3 printed template. As 3D printing resolution improves and becomes more affordable, the method should be generalizable and smaller features should be properly transferred.

Time/cost assessment

The described rapid prototyping pipeline offers significant time and cost benefits compared to conventional PDMS prototyping methods. The equipment required for this process is more readily available and/or inexpensive compared to sophisticated microfabrication tools. SLA 3D printers with excellent print resolution are now commercially available in the price range of $100 s–$1000 s. Other requisite capital equipment, such as a vacuum system, centrifuge, and oven, are commonly found in research settings. The material cost breakdown of the prototyping method compared to soft lithography can be found in SI: Table S2. The per-device material cost for all combined steps remained under $15, representing at least a tenfold reduction compared to standard soft lithography and other proposed methods[44]. We anticipate that multilayer photolithography would incur even

higher manufacturing costs due to its requirement for multiple photomasks, and the complexity of the process often leads to additional expenses, resulting from extended usage fees for microfabrication facility, besides failed iterations.

The described protocol not only offers minimal time constraints but also demonstrates efficiency. Additionally, the time constraints are relatively minimal with this described protocol. When executed sequentially, it takes less than 48 h to convert initial geometry ideation to the final product, with only 2.5 h of labor time (SI: Table S3). The majority of the 48 h manufacturing duration is attributed to idle time, involving automated 3D printing and epoxy curing. Even the brief active steps required are not technically challenging. In contrast, a significant time constraint of soft lithography involves waiting for the delivery of photomasks. Additionally, photolithography is a lengthy and technically complex process conducted by skilled personnel in cleanroom facilities. In comparison, all steps of this protocol may be completed in-house. The significant time reduction compared to standard soft lithography is a result of the optimization of each step, which could otherwise take several days.

Validation of capillaric circuits

CCs were selected to demonstrate the feasibility of the described rapid prototyping workflow. The plasma treatment of the PMMA features was necessary to create hydrophilic surfaces for achieving designed fluid flow[11]. Plasma-treated PMMA maintains its hydrophilicity over weeks, and if an alternative method for treating PMMA or preserving PMMA hydrophilicity for longer durations is desired, additional polymer coatings[55,56] or UV treatment[57,58] can be implemented. The contact angle of water on the tape and plasma-treated PMMA were experimentally determined to be 85° and 41°, respectively. The tape was precisely cut into the pre-determined size (23 mm × 40 mm) such that the inlet wells and capillary pump outlet via holes were accessible for loading solutions using pipettes. An exposed capillary pump outlet for wicking (Fig. 3A) was critical in triggering the assay. Overhanging tape made it more difficult to have the filter paper contact the solution for wicking. To further simplify the operation of the device, cutting the wicking paper to have a pointed edge allows easy placement, ensuring contact with the square, 200 µm capillary pump outlet.

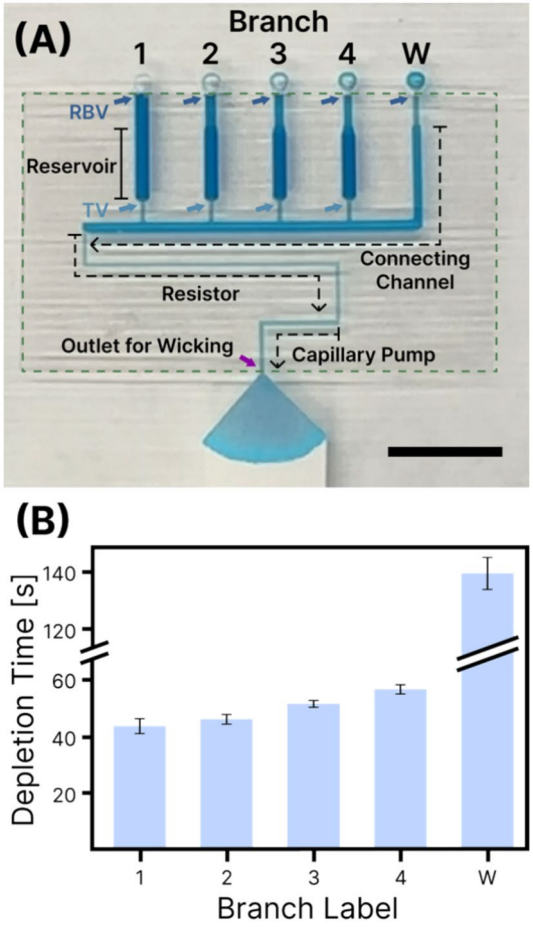

Figure 3. Demonstration of pre-programmed flow manipulation within the designed CC. (**A**) A single device fully loaded with diluted food dye at the instance when flow out of Branch 1 was initiated. CC components and features of interest are labeled. The neck of the RBV and TV are denoted by the dark and light blue arrows, respectively. The transparent sealing tape is outlined in green. Scale bar = 1 cm. (**B**) Plot of branch depletion time (n = 18) after all the solutions were loaded, prior to depletion of Branch 1.

A CC was designed with 4 sequentially flowing branches (Branches 1 through 4) alongside the wetting channel (Branch W) (Fig. 3A). After completely loading Branches 1–4 (RBV, Reservoir, and TV), fluid did not dispense into the main channel, validating the successful implementation of the TV. After adding the wetting solution to the wetting branch, the resistor and capillary pump outlet were filled with the solution. Placing the filter paper at the pump wicking outlet initiated sequential branch depletion, dependent on the sequence of RBV cross section (SI: Video S1). Branches depleted in descending order of cross-sectional area of its corresponding RBV. The average depletion time for Branches 1–4 to transport the volume of the solution from the reservoirs ranged between 40 and 50 s. (Fig. 3B). The depletion time for these branches is determined by tracking the movement of the tailing edge of the flow from the neck of RBV to the neck of TV (Fig. 3A). The wetting branch, which did not have a TV, had a slower flow time. The flow of the wetting branch was defined as the trailing edge of the solution moving from its neck of RBV and through the connecting channel, extending up to the exit of the resistor.

Immunofluorescence protein quantification assay

As a proof of concept, a simple, immunofluorescence assay was performed on-chip to quantify protein concentrations in solution. Biotinylated anti-BSA antibodies were conjugated with streptavidin-coated agarose beads before being loaded into the CC to form a reaction pack bed, providing ample surface area and excellent binding capacity for protein-specific immobilization[59,60]. Then, Branch 1 was loaded with a fluorescent BSA-FITC solution spanning a multiple order of magnitudes in concentration (100 ng/mL–1 mg/mL) while the remaining branches were loaded with 25 µL total wash buffer. This represents sequential triple washes of ~ 8 µL each to remove excess unbound protein (Fig. 4A). Loading the resuspended bead solution into the wetting branch induced the start of the on-chip flow. The 40–165 µm agarose beads in solution aggregated and compacted into a dense column in the straight channel, feeding into the 150 µm resistor channel (Fig. 4A). The bead column did not impede predicted and tested preprogrammed flow operation duration or sequence. The concentration of beads was tuned (~ 250 beads/µL) to ensure that the bead column, forming effective reaction packed bed, did not extend past the TV of Branch 1 (< 5 mm from the exit of the connecting channel, leading to the resistor). Experimentally, an excessively long column disrupted the flow and caused the branches to flow out of order.

After triggering CC fluid flow, the beads acted as the assay substrate for affinity-based protein quantification through immunofluorescence intensity. Following fluid flow, the bead column was imaged using the appropriate filter set. Serial protein dilutions were quantified via fluorescence of antibody-coated beads accumulated on the device to assess the limit of detection. Fluorescence intensity analysis of the beads post-assay completion is shown in Fig. 4B. A four-parameter logistic equation was calculated[38] to fit the serial dilution fluorescence intensities to a standard S curve[37]. The LOD was estimated to be 500 ng/mL using the negative control and minimum tested concentration fluorescence intensities[39]. If desired, additional branches and reagents may be added to further increase the sensitivity of detection or complexity of the assay[12,13,15,18].

Conclusion

We have presented a rapid and cost-effective pipeline for prototyping thermoplastic microfluidic devices. We utilized an SLA 3D printer to mold devices with complex geometries, which are then transferred to PMMA through intermediate steps involving PDMS and epoxy moldings. The efficacy of this pipeline was demonstrated

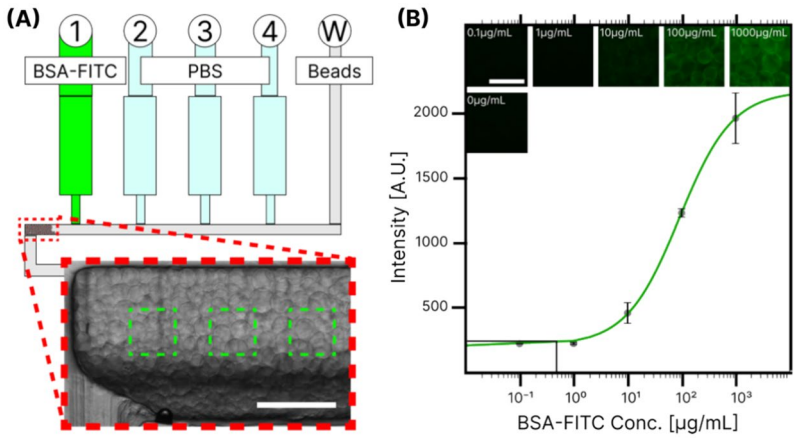

Figure 4. A proof-of-concept, automated, quantitative immunofluorescence protein quantification using antibody-coated beads in the designed CC. (**A**) A schematic representation of different reagents loaded into the CC. Inset (in red): a brightfield image of the channel with the compacted bead column. Regions of interest for fluorescence analysis are boxed in green. Note: to match the orientation of the image with the schematic, the image was inverted horizontally. Scale bar = 500 µm. (**B**) Plot comparing the mean fluorescence intensity of predetermined regions of interest (N = 3, green dotted boxes in (A)) across different devices testing various BSA-FITC concentrations. The calculated LOD (500 ng/mL) was plotted with black lines. Representative fluorescence images for each protein concentration are depicted above the plot. Scale bar = 200 µm.

by the successful fabrication and iteration of CC designs, leading to the development of a proof-of-concept bioassay. The process is compatible with various 3D printers, allowing for tradeoffs in price, print size, and resolution. Similarly, the method is transferrable to other types of thermoplastics with a simple and inexpensive hot embossing process optimization. With this process, ideas may transition from CAD files to a plastic product in less than 48 h, most of which is idle time. The total material costs for the entire manufacturing process are kept under $15, processes may be completed outside of a well-maintained microfabrication cleanroom, and requisite equipment are already largely available in research labs.

The fabrication method will be crucial for iterating on channel design using appropriate materials capable of scaled-up production. This prototyping method enables testing required chemical or other biological assay conditions directly with the material to be utilized for massive production, eliminating the need for additional re-optimization of designed assays. After iterating through designs with this method, the finalized epoxy mold may be converted into a metal mold for robust, long-term thermoplastic forming. Depending on the application and final device requirements, PMMA devices can be sealed to other thermoplastics using thermal or solvent bonding instead of tape[54,61–64]. Future works will focus on exploring other biologically relevant assays that could not be realized through conventional lateral flow assays but would benefit from inexpensive, decentralized platforms. In all, this pipeline reveals new possibilities for rapid prototyping of microfluidic devices and provides a foundation for further advancement in the field.

Data availability

Experimental data is available upon reasonable request.

Received: 20 March 2024; Accepted: 26 July 2024
Published online: 31 July 2024

References

1. Lantada, A. D. & Morgado, P. L. Rapid prototyping for biomedical engineering: Current capabilities and challenges. *Annu. Rev. Biomed. Eng.* **14**, 73–96 (2012).
2. Gupta, A. & Singh, V. A review of emerging technologies for rapid prototyping. *AIP Conf. Proc.* **2723**, 020004 (2023).
3. Xia, Y. & Whitesides, G. M. Soft lithography. *Annu. Rev. Mater. Sci.* **28**, 153–184 (1998).
4. Yang, Y., Chen, Y., Tang, H., Zong, N. & Jiang, X. Microfluidics for biomedical analysis. *Small Methods* **4**, 1900451 (2020).
5. Aubry, G., Lee, H. J. & Lu, H. Advances in microfluidics: Technical innovations and applications in diagnostics and therapeutics. *Anal. Chem.* **95**, 444–467 (2023).
6. Nguyen, N.-T., Wereley, S. T. & Shaegh, S. A. M. *Fundamentals and Applications of Microfluidics* 3rd edn. (Artech House, 2019).
7. Reyes, D. R. *et al.* Accelerating innovation and commercialization through standardization of microfluidic-based medical devices. *Lab Chip* **21**, 9–21 (2021).
8. Gong, M. M. & Sinton, D. Turning the page: Advancing paper-based microfluidics for broad diagnostic application. *Chem. Rev.* **117**, 8447–8480 (2017).
9. Nishat, S., Jafry, A. T., Martinez, A. W. & Awan, F. R. Paper-based microfluidics: Simplified fabrication and assay methods. *Sens. Actuators B Chem.* **336**, 129681 (2021).
10. Safavieh, R. & Juncker, D. Capillarics: Pre-programmed, self-powered microfluidic circuits built from capillary elements. *Lab Chip* **13**, 4180–4189 (2013).
11. Olanrewaju, A., Beaugrand, M., Yafia, M. & Juncker, D. Capillary microfluidics in microchannels: From microfluidic networks to capillaric circuits. *Lab Chip* **18**, 2323–2347 (2018).
12. Karamzadeh, V., Sohrabi-Kashani, A., Shen, M. & Juncker, D. Digital manufacturing of functional ready-to-use microfluidic systems. *Adv. Mater.* https://doi.org/10.1002/adma.202303867 (2023).
13. Yafia, M. *et al.* Microfluidic chain reaction of structurally programmed capillary flow events. *Nature* **605**, 464–469 (2022).
14. Achille, C. *et al.* 3D printing of monolithic capillarity-driven microfluidic devices for diagnostics. *Adv. Mater.* **33**, 2008712 (2021).
15. Parandakh, A. *et al.* 3D-printed capillaric ELISA-on-a-chip with aliquoting. *Lab Chip* **23**, 1547–1560 (2023).
16. Azizian, P. *et al.* Coupling capillary-driven microfluidics with lateral flow immunoassay for signal enhancement. *Biosensors* **13**, 832 (2023).
17. Yan, S. *et al.* A rapid, maskless 3D prototyping for fabrication of capillary circuits: Toward urinary protein detection. *ELECTROPHORESIS* **39**, 957–964 (2018).
18. Azizian, P., Casals-Terré, J., Ricart, J. & Cabot, J. M. Diffusion-free valve for preprogrammed immunoassay with capillary microfluidics. *Microsyst. Nanoeng.* **9**, 1–13 (2023).
19. Makhinia, A. *et al.* On-demand inkjet printed hydrophilic coatings for flow control in 3D-printed microfluidic devices embedded with organic electrochemical transistors. *Adv. Mater. Technol.* **8**, 2300127 (2023).
20. Olanrewaju, A. O., Ng, A., DeCorwin-Martin, P., Robillard, A. & Juncker, D. Microfluidic capillaric circuit for rapid and facile bacteria detection. *Anal. Chem.* **89**, 6846–6853 (2017).
21. Battat, S., Weitz, D. A. & Whitesides, G. M. An outlook on microfluidics: The promise and the challenge. *Lab Chip* **22**, 530–536 (2022).
22. Volpatti, L. R. & Yetisen, A. K. Commercialization of microfluidic devices. *Trends Biotechnol.* **32**, 347–350 (2014).
23. Cong, H. & Zhang, N. Perspectives in translating microfluidic devices from laboratory prototyping into scale-up production. *Biomicrofluidics* **16**, 021301 (2022).
24. Becker, H. It's the economy.… *Lab Chip* **9**, 2759–2762 (2009).
25. Nielsen, A. V., Beauchamp, M. J., Nordin, G. P. & Woolley, A. T. 3D printed microfluidics. *Annu. Rev. Anal. Chem.* **13**, 45–65 (2020).
26. Gonzalez, G., Roppolo, I., Pirri, C. F. & Chiappone, A. Current and emerging trends in polymeric 3D printed microfluidic devices. *Additive Manuf.* **55**, 102867 (2022).
27. Gale, B. K. *et al.* A review of current methods in microfluidic device fabrication and future commercialization prospects. *Inventions* **3**, 60 (2018).
28. Tsao, C.-W. Polymer microfluidics: Simple, low-cost fabrication process bridging academic lab research to commercialized production. *Micromachines* **7**, 225 (2016).
29. Lee, U. N. *et al.* Fundamentals of rapid injection molding for microfluidic cell-based assays. *Lab Chip* **18**, 496–504 (2018).
30. Lin, T.-Y., Do, T., Kwon, P. & Lillehoj, P. B. 3D printed metal molds for hot embossing plastic microfluidic devices. *Lab Chip* **17**, 241–247 (2017).
31. Sollier, E., Murray, C., Maoddi, P. & Di Carlo, D. Rapid prototyping polymers for microfluidic devices and high pressure injections. *Lab Chip* **11**, 3752 (2011).

32. Olanrewaju, A. O., Robillard, A., Dagher, M. & Juncker, D. Autonomous microfluidic capillaric circuits replicated from 3D-printed molds. *Lab Chip* **16**, 3804–3814 (2016).
33. Stalder, A. F., Kulik, G., Sage, D., Barbieri, L. & Hoffmann, P. A snake-based approach to accurate determination of both contact points and contact angles. *Colloids Surf. A Physicochem. Eng. Asp.* **286**, 92–103 (2006).
34. Schindelin, J. *et al.* Fiji: An open-source platform for biological-image analysis. *Nat. Methods* **9**, 676–682 (2012).
35. Compare Formlabs SLA 3D Printer Tech Specs. *Formlabs* https://formlabs.com/3d-printers/form-3/tech-specs/.
36. Venzac, B. *et al.* PDMS curing inhibition on 3D-printed molds: Why? Also, how to avoid it?. *Anal. Chem.* **93**, 7180–7187 (2021).
37. Karpinski, K. F., Hayward, S. & Tryphonas, H. Statistical considerations in the quantitation of serum immunoglobulin levels using the enzyme-linked immunosorbent assay (ELISA). *J. Immunol. Methods* **103**, 189–194 (1987).
38. AAT Bioquest, Inc. Four Parameter Logistic (4PL) Curve Calculator. (2024).
39. Armbruster, D. A. & Pry, T. Limit of blank, limit of detection and limit of quantitation. *Clin. Biochem. Rev.* **29**, S49–S52 (2008).
40. Kim, M., Moon, B.-U. & Hidrovo, C. H. Enhancement of the thermo-mechanical properties of PDMS molds for the hot embossing of PMMA microfluidic devices. *J. Micromech. Microeng.* **23**, 095024 (2013).
41. Maurya, D. K., Ng, W. Y., Mahabadi, K. A., Liang, Y. N. & Rodríguez, I. Fabrication of lab-on chip platforms by hot embossing and photo patterning. *Biotechnol. J.* **2**, 1381–1388 (2007).
42. Goral, V. N., Hsieh, Y.-C., Petzold, O. N., Faris, R. A. & Yuen, P. K. Hot embossing of plastic microfluidic devices using poly(dimethylsiloxane) molds. *J. Micromech. Microeng.* **21**, 017002 (2011).
43. Qin, Y. *et al.* A reinforced PDMS mold for hot embossing of cyclic olefin polymer in the fabrication of microfluidic chips. *Lab Chip* **22**, 4729–4734 (2022).
44. Young, E. W. K. *et al.* Rapid prototyping of arrayed microfluidic systems in polystyrene for cell-based assays. *Anal. Chem.* **83**, 1408–1417 (2011).
45. Jena, R. K., Yue, C. Y., Lam, Y. C., Tang, P. S. & Gupta, A. Comparison of different molds (epoxy, polymer and silicon) for micro-fabrication by hot embossing technique. *Sens. Actuators B Chem.* **163**, 233–241 (2012).
46. Koerner, T., Brown, L., Xie, R. & Oleschuk, R. D. Epoxy resins as stamps for hot embossing of microstructures and microfluidic channels. *Sens. Actuators B Chem.* **107**, 632–639 (2005).
47. Fiorini, S., Jeffries, G. D. M., Lim, D. S. W., Kuyper, C. L. & Chiu, D. T. Fabrication of thermoset polyester microfluidic devices and embossing masters using rapid prototyped polydimethylsiloxane molds. *Lab Chip* **3**, 158–163 (2003).
48. Mehta, G. *et al.* Hard top soft bottom microfluidic devices for cell culture and chemical analysis. *Anal. Chem.* **81**, 3714–3722 (2009).
49. Svoboda, M., Schrott, W., Slouka, Z., Přibyl, M. & Šnita, D. Plastic microfluidic systems made by imprinting against an epoxy stamp. *Microelectron. Eng.* **87**, 1527–1530 (2010).
50. Shaegh, S. A. M. *et al.* Rapid prototyping of whole-thermoplastic microfluidics with built-in microvalves using laser ablation and thermal fusion bonding. *Sens. Actuators B Chem.* **255**, 100–109 (2018).
51. LeMon, M. B., Douma, C. C., Burke, G. S. & Bowser, M. T. Fabrication of µFFE devices in COC via hot embossing with a 3D-printed master mold. *Micromachines* **14**, 1728 (2023).
52. Comina, G., Suska, A. & Filippini, D. PDMS lab-on-a-chip fabrication using 3D printed templates. *Lab Chip* **14**, 424–430 (2014).
53. Waheed, S. *et al.* Enhanced physicochemical properties of polydimethylsiloxane based microfluidic devices and thin films by incorporating synthetic micro-diamond. *Sci. Rep.* **7**, 15109 (2017).
54. Brown, L., Koerner, T., Hugh Horton, J. & Oleschuk, D. R. Fabrication and characterization of poly (methylmethacrylate) micro-fluidic devices bonded using surface modifications and solvents. *Lab Chip* **6**, 66–73 (2006).
55. Yu, H., Chong, Z. Z., Tor, S. B., Liu, E. & Loh, N. H. Low temperature and deformation-free bonding of PMMA microfluidic devices with stable hydrophilicity via oxygen plasma treatment and PVA coating. *RSC Adv.* **5**, 8377–8388 (2015).
56. Bi, H. *et al.* Deposition of PEG onto PMMA microchannel surface to minimize nonspecific adsorption. *Lab Chip* **6**, 769–775 (2006).
57. Lin, T.-Y., Pfeiffer, T. T. & Lillehoj, P. B. Stability of UV/ozone-treated thermoplastics under different storage conditions for micro-fluidic analytical devices. *RSC Adv.* **7**, 37374–37379 (2017).
58. Bae, G., Park, T. & Song, I.-H. Surface modification of polymethylmethacrylate (PMMA) by ultraviolet (UV) irradiation and IPA rinsing. *Micromachines* **13**, 1952 (2022).
59. Cuatrecasas, P. Protein purification by affinity chromatography: Derivatizations of agarose and polyacrylamide beads. *J. Biol. Chem.* **245**, 3059–3065 (1970).
60. Costa, S. P. *et al.* A microfluidic platform combined with bacteriophage receptor binding proteins for multiplex detection of *Escherichia coli* and *Pseudomonas aeruginosa* in blood. *Sens. Actuators B Chem.* **376**, 132917 (2023).
61. Bamshad, A., Nikfarjam, A. & Khaleghi, H. A new simple and fast thermally-solvent assisted method to bond PMMA–PMMA in micro-fluidics devices. *J. Micromech. Microeng.* **26**, 065017 (2016).
62. Mair, D. A. *et al.* Room-temperature bonding for plastic high-pressure microfluidic chips. *Anal. Chem.* **79**, 5097–5102 (2007).
63. Zhu, X., Liu, G., Guo, Y. & Tian, Y. Study of PMMA thermal bonding. *Microsyst. Technol.* **13**, 403–407 (2007).
64. Faghih, M. M. & Sharp, M. K. Solvent-based bonding of PMMA–PMMA for microfluidic applications. *Microsyst. Technol.* **25**, 3547–3558 (2019).

Acknowledgements

The authors would like to acknowledge Huy Vo and the Whiting School of Engineering Whitaker Microfabrication Lab for facility guidance, Dr. Paul Haghi Ashtiani and the Material Characterization and Processing Facility for imaging assistance, and Dr. Srivathsan Kalyan for help with process optimization. We acknowledge funding from the Gordon and Betty Moore Foundation, the Space@Hopkins Initiative, the J&J WiSTEM^{2}D Scholars Award and NCI IMAT grant (R21CA229024).

Author contributions

H.K. conceptualized, developed and investigated the methodology, performed data analyses, and wrote the manuscript. W.S.A. assisted with experimental investigation. N.A.C. provided experimental resources. S.C.H. conceptualized, supervised the research development and data analysis, and wrote the manuscript. All authors contributed to manuscript writing.

Competing interests

The authors declare no competing interests.

Additional information

Supplementary Information The online version contains supplementary material available at https://doi.org/10.1038/s41598-024-68761-5.

Correspondence and requests for materials should be addressed to S.C.H.